

The Effects of Mold Design on the Pore Morphology of Polymers Produced with MuCell[®] Technology

HONGBIN WU* AND ERICH WINTERMANTEL

*Department and Chair for Medical Engineering, TU München,
Boltzmannstr.15, 85748 Garching, Germany*

HÅVARD J. HAUGEN

*Department of Biomaterials, Institute for Clinical Dentistry,
University of Oslo, PO Box 1109 Blindern, 0317 Oslo, Norway*

ABSTRACT: In this study two molds were designed and used in MuCell[®] technology to generate implants with a porous structure. To arrive the desired pore structure many process parameters were investigated for indicating the effects of process parameters on the pore morphology. This process parameter investigation was performed on each mold respectively, so that the influences of the mold design on the pore morphology have been researched by the same process parameter setting. It was found that the mold design also had effects on the pore structure in MuCell[®] technology. A proper mold design could improve the generated pore structure, such as porosity, pore diameter, and interconnectivity.

KEY WORDS: mold design, cell morphology, MuCell[®], injection molding, medical implant, porous polymer, polyurethane.

*Author to whom correspondence should be addressed.
E-mail: gilbert.whb@gmail.com
Figure 2 appears in color online: <http://cel.sagepub.com>

INTRODUCTION

MuCell[®] technology, as an effective microcellular injection molding process, is widely used in automobile and furniture industries. In most cases, MuCell[®] technology is used to save raw materials, but it is also used to produce implants with closed porous structure [1]. It uses CO₂ as blowing agent, which is injected in the plasticization section of the injection molding machine (Figure 1). The blowing agent is injected into the polymer melt through the gas supply line and injector, in its super critical state, by the plasticization phase of the injection molding machine. After the plasticization the mixture of polymer melt and gas is injected through the nozzle into the mold, where the foam structure can be generated due to the quick pressure drop in the mold. The main products which are produced today with MuCell[®] technology have closed cellular foam [2–4].

Some studies have investigated the relations between the key process parameters in MuCell[®] technology and produced cellular foam structure [1,5,6]. It was found that the pore morphology in MuCell[®] process could be adjusted through varying the process parameters. However, there is currently no literature regarding the effects of mold design on the pore morphology by MuCell[®] technology.

In this study two molds were designed and used in MuCell[®] process to generate implants with a porous structure for medical use. The research of process parameters was independently performed on these two molds. By comparing the pore structure of implants made from two molds at the same process parameter setting, the influences of the mold design on the porous structure were investigated.

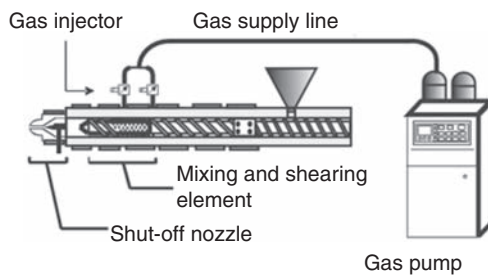


Figure 1. Draft of the MuCell[®] technology (figure according to [12]).

MATERIALS AND METHODS

Polymer Processing

Medical grade thermoplastic polyurethane TPU (Texin[®] 985, Bayer, Pa, USA) was chosen as raw material for the implant. An injection molding machine (KM 125-520C2, KraussMaffei Technologies GmbH, Munich, Germany) with a temperature control unit for cooling the mold (90S/6/TS22/1K/RT45, Regloplas, St. Gallen, Switzerland) was used for the production of the samples. The injection molding machine was equipped with a MuCell[®] package by the Trexel Inc., Woburn, MA, USA. The MuCell[®] package is schematically shown in Figure 1. The blowing agent is injected into the polymer melt through the gas supply line and injector, in its super critical state, by the plasticization phase of the injection molding machine. After the plasticization the mixture of polymer melt and gas is injected through the nozzle into the mold, where the foam structure can be generated due to the quick pressure drop in the mold.

CO₂ was used as blowing agent (CO₂ protective gas DIN-32525-C1, Westfalen AG, Münster, Germany).

In order to produce the implant, two particular molds were designed and used. The technical drawings of molded parts from mold A and mold B are shown in Figure 2. The mold A had six ring shaped implants and was just used for the preliminary test of the feasibility of the foaming process and parameter research. The mold B was designed with six solid disk shaped implant based on the results of *in vivo* test of implants from mold A, for a higher biological requirement and prospective production.

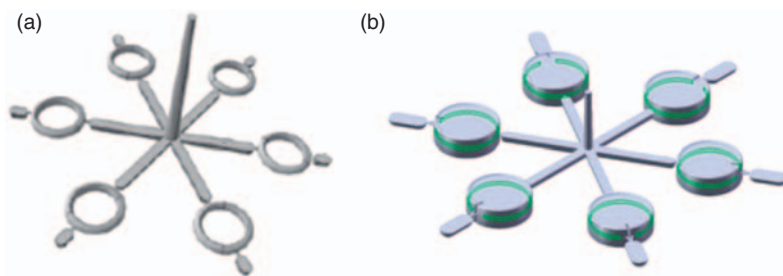


Figure 2. Different mold designs.

Two molds have similar gate, runner, and sprues. The mold B has a shorter polymer melt flow of mold cavity and the L/D (length/thickness) of 2.8, whereas this L/D for mold A is 4.7. This means the molded part from mold B is relatively thicker but shorter. The advantage of mold B is that the energy loss of melt flow, which dominates the cell nucleation and growth, is reduced due to the shorter flow path (low L/D). As a result better pore morphology, such as bigger mean pore size, higher porosity, and so on, could be expected. On the other hand the mold B has a bigger capacity which means more possibilities of parameter variation. The disadvantage of mold B is that relative thicker molded part will lead to an incomplete filling of the cavity of mold B, a long cooling time, and significant shrinkage of molded part, in normal injection molding process. These problems could be partially or wholly resolved if the foaming process is applied due to the expansion of foamed polymer.

Experimental Strategy

The choice of the changeable parameters was made based on the knowledge given by nucleation theory and literature search [5,7]. The ranges of variable parameters and the values of fixed parameters are presented in Table 1. The experiments were done by varying one of

Table 1. Ranges of variable parameters and values of fixed parameters of the MuCell[®] process in this study. The microcellular process pressure (MPP) is an active pressure that keeps the gas in polymer melt. This pressure is actually the plasticizing pressure.

Variable parameters	Examined range
CO ₂ concentration	1–6 wt%
Degree of weight reduction	35–65%
Injection speed	30–300 mm/s
Plasticizing pressure/MPP	160–220 bar
Plasticizing temperature	180–210°C
Mold temperature	25–85°C
Fixed parameters	Value
Cooling time	120 s
Dwell pressure	450 bar
Beginning dwell pressure	0.5 mm
Duration of dwell pressure	0.5 s
Clamp tonnage	200 kN
Plasticizing rotation	40 min ⁻¹
Injection pressure	0–3000 bar

variable parameters while keeping the others constant. The whole process parameters investigation was performed on two molds respectively. The implants from two molds, which were used to be compared, were produced at exactly same process parameters, so that the effects of different molds were shown.

Characterization of Macro- and Microstructures

Scanning electron microscopy (SEM; Jeol JSM-6060LV, JEOL Ltd., Tokyo, Japan) was used for the observation of the pore morphology of the cross section of implant. The samples were sliced with a scalpel and then coated with a thin gold layer by using a sputter-coater (SCD 005, BAL-TEC AG, Balzers, Lichtenstein) under high vacuum with a voltage range between 5 and 15 kV. Characteristics of porous structure such as pore size and porosity can be calculated by counting the average cell number and size of several SEM-images from one sample.

One cut area with certain size was chosen and all pores were measured manually with the help of software of digital microscope (VHX-500, Keyence Corporation, Osaka, Japan). The average diameter of pores was calculated as D_{measured} . Due to the fact that the pores shown in the micrographs are 2D projections of 3D objects, their maximum diameter may not be represented in the image. Following equation was used for determination of the maximum spherical diameter, named corrected median pore diameter, from the measured pore diameter: [1].

$$D_{\text{Corr}} = \frac{D_{\text{measured}}}{0.616} \quad (1)$$

MicroCT (SkyScan 1172, SkyScan, Kontich, Belgium) was used to quantitatively measure the porous interconnectivity of implants – three 8 mm × 11 mm cylindrical samples from each implant ($n=3$) at 7 μm resolution using a voltage of 59 kV, and a current of 167 μA. Image reconstruction and analysis were conducted using the software package provided by SkyScan. Samples were rotated 180° around their long axis and three absorption images were recorded every 0.400° of rotation. These raw images of the samples were reconstructed with the standard SkyScan reconstruction software (NRecon) to serial coronal-oriented tomograms using 3D cone beam reconstruction algorithm. For the reconstruction, beam hardening was set to 20% and ring artefact reduction to 12.

The image analysis of the reconstructed axial bitmap images was performed using the standard SkyScan software (CTan and CTvol).

First, a thresholding analysis was performed to determine the threshold value for which the greyscale tomograms of scaffolds were most accurately represented by their binarised counterparts in terms of porosity. The threshold value was set between 65 and 225 for this study. Additional noise was removed by the ‘despeckling’ function. All objects smaller than 500 voxels and not connected to the 3D body were thus removed prior to further analysis. In order to eliminate potential edge effects, a cylindrical volume of interest (VOI) with a diameter of 5 mm and a height of 2.5 mm was selected in the centre of the scaffold. Scaffold porosity was then calculated as follows:

$$\text{Porosity} = 100\% - \text{vol. \% of binarised object (scaffold materials) in VOI} \quad (2)$$

All images underwent 3D analysis, followed by the quantification of interconnectivity using the ‘shrink-wrap’ function, which allows measuring the fraction of pore volume in a scaffold that was accessible from the outside through openings of a certain minimum size [8]. A shrink-wrap process was performed between two 3D measurements to shrink the outside boundary of the VOI in a scaffold through openings the size of which was equal to or larger than a threshold value (0–280 μm were used in this study). Interconnectivity was calculated as follows:

$$\text{Interconnectivity} = \frac{V - V_{\text{shrink-wrap}}}{V - V_m} \times 100\%, \quad (3)$$

where V is the total volume of VOI, $V_{\text{shrink-wrap}}$ is the VOI volume after shrink-wrap processing, and V_m is the volume of scaffold material.

RESULTS AND DISCUSSION

The SEM images (Figure 3) show the pore structures of foamed implants from two molds in the injection speed variation with value of 30 mm/s, when the other process parameters were kept unchanged (weight reduction of 35%, plasticizing temperature of 180°C, plasticizing pressure of 180 bar, mold temperature of 25°C, and gas content of 2%). It was found that the left image, which came from the foamed implant from mold B, showed a significant larger pore size than right image from mold A. The interconnective pore size [9,10] which means the window between two connective pores has also the same change trend. From Figure 3 it could be qualitatively seen that the implants from mold B had a larger pore size and interconnective pore size and possibly had a higher porosity than those from mold A at the same process parameter.

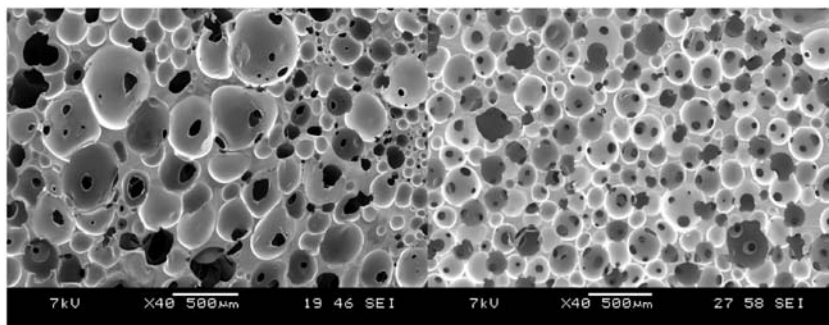


Figure 3. Different pore structures of mold B (left) and mold A (right) at the injection speed of 30 mm/s.

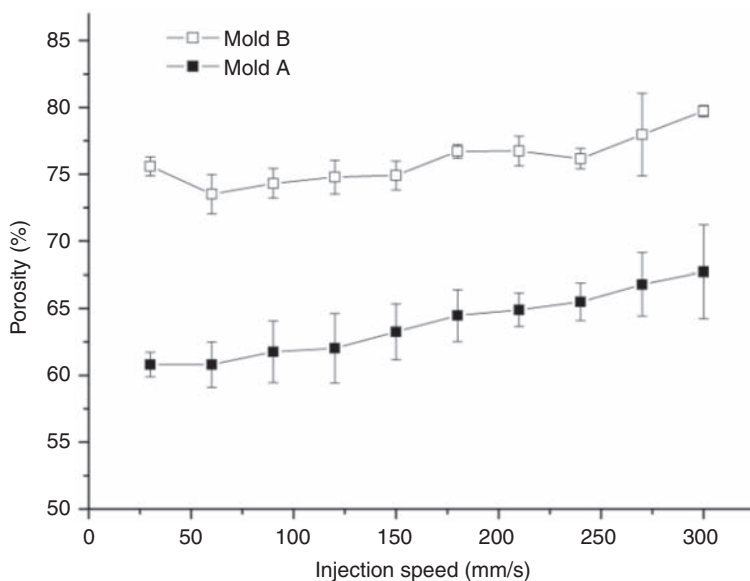


Figure 4. Differences of the porosity at injection speed variation.

It was found from Figure 4 that the implants from mold B at every different injection speed had a higher porosity than the implants from mold A. The porosity range of implants from mold B was between 73% and 79%, whereas by mold A this porosity range was between 60% and 67%. At the same time the standard deviation of the porosity from mold B was significantly smaller than the deviation by mold A.

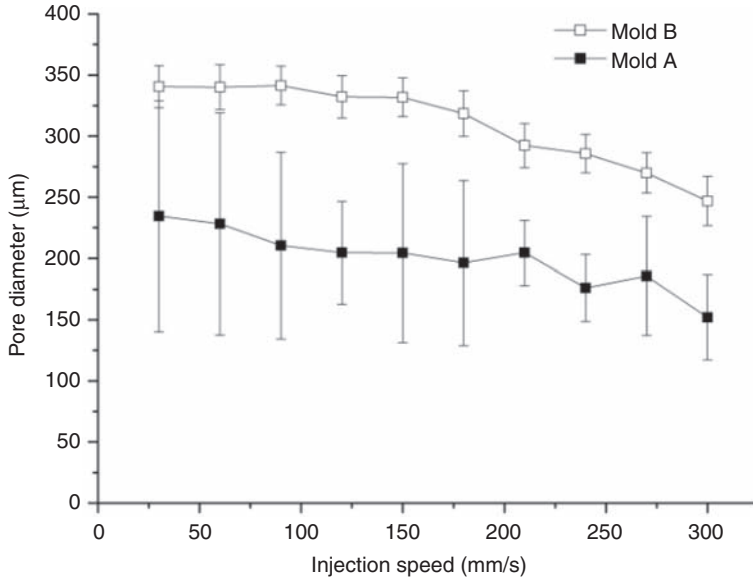


Figure 5. The mean pore size from two molds at different injection speeds.

Figure 5 shows the mean pore size of two molds by different injection speeds. The pore size decreased with rise of the injection speed for two molds. The same result was also found by other study [11]. The pore diameter of the implants from mold B decreased from $340 \pm 17 \mu\text{m}$ to $246 \pm 20 \mu\text{m}$ with injection speed increase; the mold A showed the pore diameter from $234 \pm 90 \mu\text{m}$ to $152 \pm 34 \mu\text{m}$ by the same injection speed variation. The mean pore size from mold B at every speed was also higher compared with mold A. It was clear that the standard deviation from mold B was also significantly smaller than the values from mold A.

Figure 6 shows the interconnective pore size of foamed implants. The interconnective pore size is very important for the tissue in growth in Biology. The interconnective pore size of foamed implants from mold B had a range of $91 \pm 6 \mu\text{m}$ to $67 \pm 7 \mu\text{m}$; by mold A this range was $35 \pm 10 \mu\text{m}$ to $19 \pm 8 \mu\text{m}$. This change was also corresponding to the finding in the mean pore size of foamed implants from two molds.

It could be concluded from Figures 3–6 that the improved mold design of mold B could not affect the change tendency of pore structure, such as decreased pore size with rise of the injection speed, but it could increase the porosity and the mean pore size as well as the interconnective pore size of the foamed implants. At the same time the standard deviation of

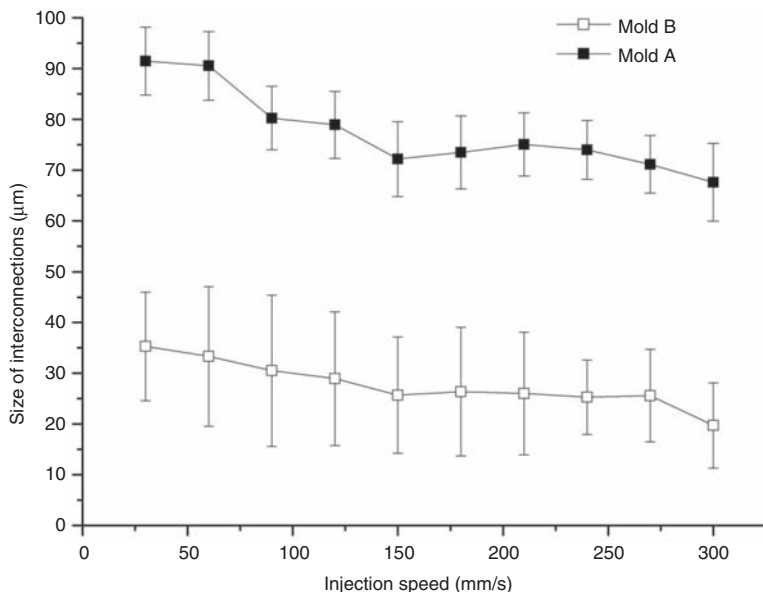


Figure 6. Size of interconnections of implants at different injection speeds.

pore structure was significantly decreased. In other words the pore structure of foamed implants from mold B had a higher porosity, a larger pore size, and was more uniform than those from mold A.

Figure 7 shows the comparison of the maximal porosity at different kinds of process parameter variations, including the injection speed, from two molds. In every kind of process parameter variations, the maximal porosity was always obtained at a same setting value for two molds, such as 79% and 67% at 300 mm/s by mold B and mold A for the injection speed variation. It was observed that mold B indicated a higher maximal porosity at every kind of parameter variation. The porosity at 35% weight reduction from mold B showed a minimal elevation of ca. 6% while the maximal porosity elevation of 14% was found by injection speed variation.

The differences between the maximal pore sizes at different kinds of process parameter variations of two molds are shown in Figure 8. Implants from two molds showed the maximal pore size also at the same process parameters setting in every kind of variation. The mold B has always a larger maximal pore size than mold A. The minimal elevation of maxima pore size of mold B was 14% by the plasticizing temperature variation, whereas the maximal elevation of pore size with value of 45% was found by the injection speed variation.

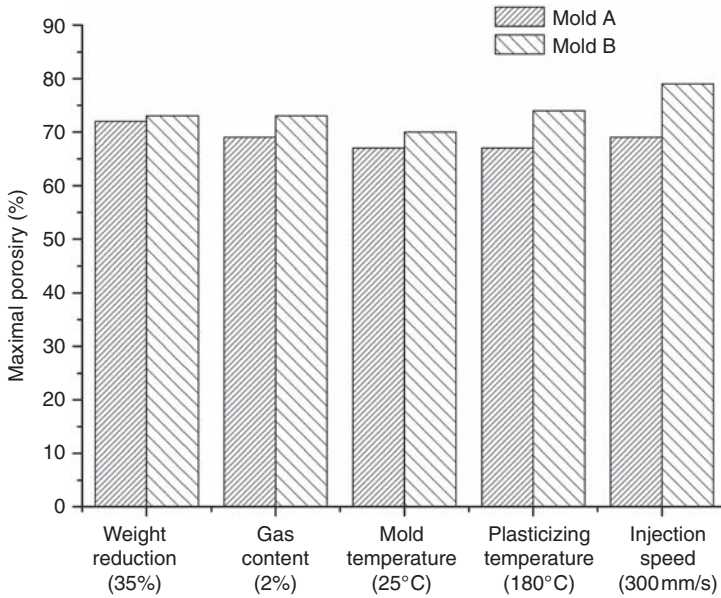


Figure 7. Differences between the maximal porosity at different processing parameters for two molds.

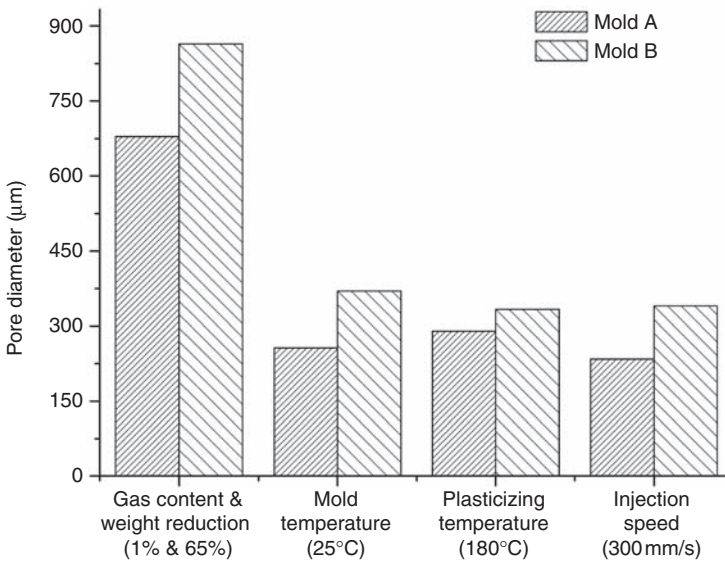


Figure 8. Differences between the maximal pore size at different process parameters for two molds.

Figure 7 and 8 have indicated that the improvement of the pore structure, such as maximal pore size and porosity, induced by the change of mold design could be observed not only in variation of the injection speed but also in all process parameters variations. The shortened L/D by mold B led to a decreased energy loss which dominates the cell nucleation, during the polymer melt flow in the mold cavity. The relative thicker implant from mold B needed also a longer cooling time, which was very important for the cell growth in the mold. Considering the possibility of interaction of these factors, using formulae of cell nucleation theory to predict the change of final pore morphology is very difficult in this study, but the effects of mold design on pore morphology such as porosity and mean pore size were successfully observed through the experiments.

CONCLUSION

This study was intent to investigate the potential effect of the mold design on the pore morphology. The improved pore morphology such as the higher porosity, larger mean pore size, and smaller deviation was found by the foamed samples from mold B. This indicated that besides the effects of process parameters, the mold design, that is, product design has also a distinct influence on the foam behavior of foaming process, which has given the possibility to improve the pore morphology through a more suitable mold design if the process parameters are limited.

The porosity and pore size are key properties for porous medical devices since cells need space in order to grow. Additionally, the pores need to be interconnected to allow the cells to migrate into the porous structure. This study showed that when producing porous medical polymer devices, appropriate mold design is a key factor for a successful device.

ACKNOWLEDGMENT

The authors acknowledge the financial support of Bayerische Forschungsstiftung with grant number AZ 639/05.

REFERENCES

1. Leicher, S., Walter, A., Schneebauer, M. et al. Molded Polystyrene Material, *Cell. Polym.*, 2006: **25**: 99–107.
2. Dassow, J. Foamed Parts with Excellent Surface Quality, *Kunstst-Plast. Eur.*, 2003: **93**: 65.

3. Rief, B. and Gundrum, J. Mikrozellulare Bauteile aus der Spritzgießmaschine, *Kunstst-Plast. Eur.*, 2003: **93**: 42–45.
4. Schonherr, O. Physical Foaming for Cost-effective Injection Moulding, *Kunstst-Plast. Eur.*, 2003: **93**: A22–A27.
5. Kawashima, H. and Shimbo, M. Effect of Key Variables on Microstructure of Injection Molded Microcellular Polystyrene Foams, *Cell. Polym.*, 2003: **22**: 175–190.
6. Wu, H., Krampe, E., Schlicht, H. and Wintermantel, E. (2009). *Application of a Microcellular Injection Molding Process (MuCell®) to Produce an Implant with Porous Structure*, Berlin, Springer Verlag.
7. Okamoto, K.T. (2003). *Microcellular Processing*, Munich, Carl Hanser Verlag.
8. Moore, M.J., Jabbari, E., Ritman, E.L. et al. Quantitative Analysis of Interconnectivity of Porous Biodegradable Scaffolds with Micro-CT, *J. Biomed. Mater. Res. A.*, 2004: **71**: 258–267.
9. Lu, J.X., Flautre, B., Anselme, K. et al. Role of Interconnections in Porous Bioceramics on Bone Recolonization *In Vitro* and *In Vivo*, *J. Mater. Sci. Mater. Med.*, 1999: **10**: 111–120.
10. Mastrogiacomo, M., Scaglione, S., Martinetti, R. et al. Role of Scaffold Internal Structure on *In Vivo* Bone Formation in Macroporous Calcium Phosphate Bioceramics, *Biomaterials*, 2006: **27**: 3230–3237.
11. Lee, J.W.S., Wang, J., Yoon, J.D. and Park, C.B. Strategies to Achieve a Uniform Cell Structure with a High Void Fraction in Advanced Structural Foam Molding, *Ind. Eng. Chem. Res.*, 2008: **47**: 9457–9464.
12. Wintermantel, E. and Ha, S.-W. (2008). *Medizintechnik*, Berlin, Springer Verlag.